Arabian Journal of Geosciences (2020) 13: 1044
https://doi.org/10.1007/s12517-020-06021-2

ORIGINAL PAPER

Hydrothermal alteration-related kaolinite/dickite occurrences in ignimbrites: an example from Miocene ignimbrite units in Avanos, Central Turkey

Murat Çiflikli[1]

Received: 24 August 2020 / Accepted: 11 September 2020 / Published online: 30 September 2020

Abstract
Miocene-Quaternary volcanic complexes associated ignimbrites from the Cappadocia Volcanic Province in Central Anatolia have been subjected to hydrothermal alteration which produced several industrial clay mineralizations. This study focuses on the hydrothermally altered Late Miocene dacitic to trachy-andesitic ignimbrites in the Avanos region and aimed to determine the alteration in terms of conditions and origin. Hydrothermally altered samples consist mainly of quartz and kaolin group clays, and minor amounts of goethite/limonite, alunite, jarosite, illite, and mixed-layered illite-smectite. The kaolinite and dickite associations were principally determined from the diagnostic XRD peaks and confirmed by FTIR and SEM data. They have fine-grained and pseudo-hexagonal uniform-kaolinite and prolonged-dickite-shaped platelets as tightly packed vermicular booklets. The kaolinite and dickite association with fine-grained alunite and jarosite point out the steam-heated igneous environments at shallow depth level. Hydrothermal alteration-related minerals occurred as replacement of volcanic glass/groundmass and neoformation in the pores from the acidic hydrothermal solutions. The mineralogical associations suggest that the hydrothermal alteration occurred in acidic and moderate temperature conditions. Major and trace element compositions of altered samples exhibit distinct differences with respect to the host-rock composition. Chondrite normalized LREE contents increase, whereas HREE contents decrease in altered ignimbrites with respect to unaltered ignimbrite. The oxygen and hydrogen isotope data of kaolinite/dickite demonstrate that magmatic vapor phases mixed with meteoric waters. The steam-heating-related igneous environment seems to be responsible for magmatic vapors which circulated along the crack zones within the acidic volcanogenic rocks, and therefore the acidic conditions caused kaolin-dominant alteration.

Keywords Avanos region · Miocene · Ignimbrite · Kaolinite · Dickite · Hydrothermal alteration

Introduction

Kaolin group minerals (kaolinite, dickite, nacrite) having 1:1 phyllosilicate structure with a composition of $Al_2Si_2O_5(OH)_4$ are common hydrothermal alteration minerals under acidic conditions, that formed by alteration of primary igneous minerals as well as direct precipitation (neoformation) from the hydrothermal fluids (e.g., Murray 1988; Murray and Keller 1993; Inoue 1995). Hydrothermal alteration of volcanic and volcanoclastic rocks with acidic and intermediate composition commonly leads to the formation of industrial clays (e.g., Murray 1988). For instance, there are several industrial kaolin deposits in volcanic-hosted rocks related to acidic conditions in several regions of Turkey (Karakaya et al. 2001; Sayın 2007; Karakaya 2009; Ece et al. 2013; Kadir and Erkoyun 2013; Kadir et al. 2014; Ünal-Ercan et al. 2016; Başıbüyük and Yalçın 2019). The study area is located in the Cappadocia Volcanic Province (CAVP) that contains Miocene-aged volcanogenic units (Innocenti et al. 1975; Temel 1992) (Fig. 1).

Previous studies on CAVP units generally focused on the tectonic, petrological, geochemical, and volcanological aspects (e.g., Innocenti et al. 1975; Schumacher et al. 1990; Le Pennec et al. 1994; Mues-Schumacher and Schumacher 1996; Schumacher and Mues-Schumacher 1996; Temel et al. 1998; Le Pennec et al. 2005; Viereck-Götte et al. 2010; Schmitt et al.

Responsible Editor: Domenico M. Doronzo

✉ Murat Çiflikli
muratc@ohu.edu.tr

[1] Department of Geological Engineering, Faculty of Engineering, Niğde Ömer Halisdemir University, 51240 Niğde, Turkey

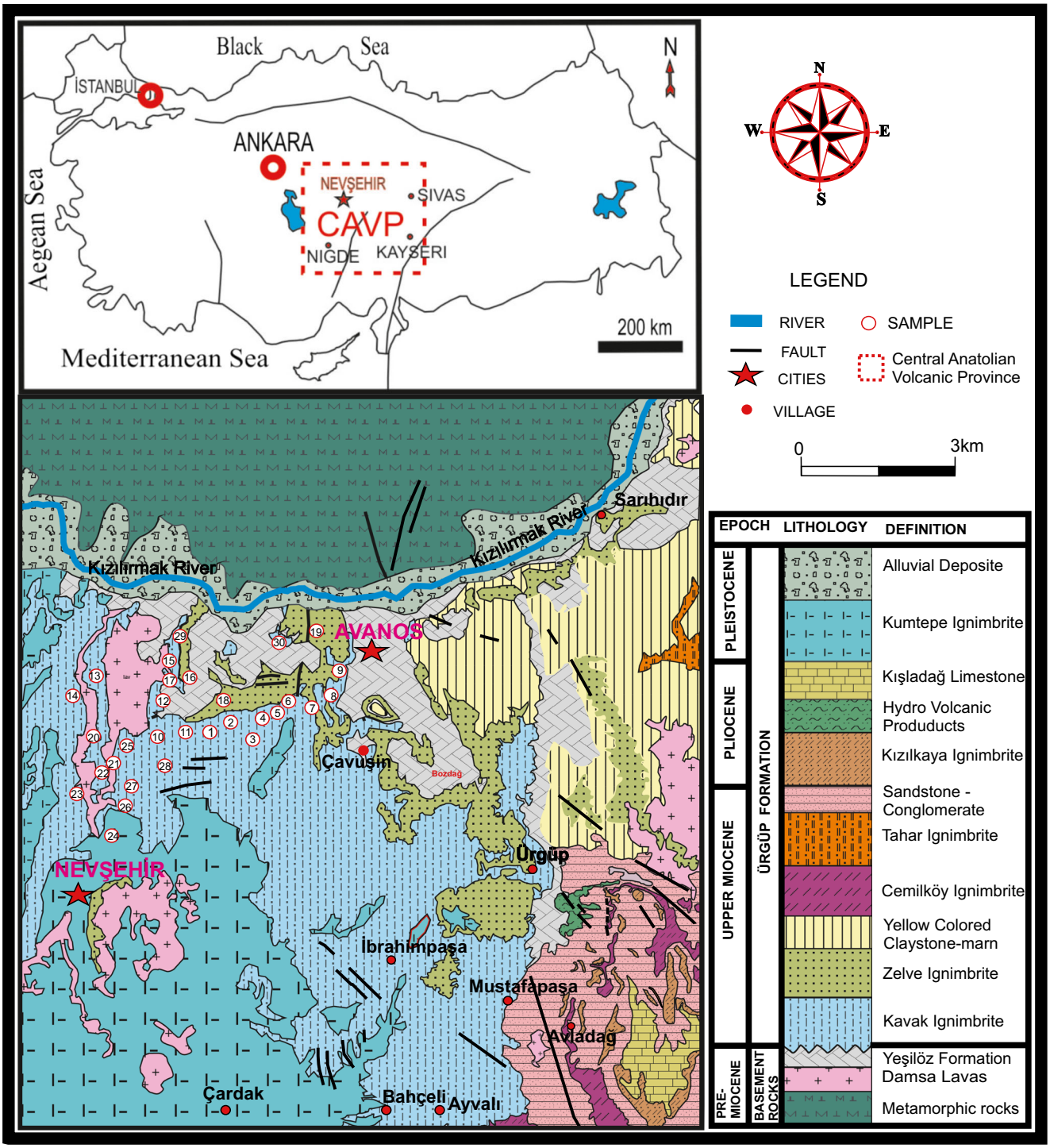

Fig. 1 Geological map and stratigraphic section of the Avanos-Nevşehir area (modified from Aydar 2012) and location of the studied samples

2011; Aydar et al. 2012) while only a few studies were made on clay occurrences in CAVP (Ertek and Öner 2008; Gurel and Kadir 2008; Kadir et al. 2013). Ertek and Öner (2008) mentioned the possible hydrothermal alteration effect on the ignimbrites and stated an intense alteration caused the kaolin clay occurrences and their industrial uses effect, but did not provide any detail for hydrothermal alteration. The origin and conditions of volcanic-hosted clay-bearing alteration can provide important data and/or tools for determining potential industrial clay occurrences for widely distributed volcaniclastic layers in CAVP. This study is focused on the hydrothermal alteration of the lowermost parts of ignimbrite beds. The Kavak ignimbrite (Pasquaré 1968) represents the earliest volcanogenic stages (9.12 Ma, Aydar et al. 2012), and its

ignimbrite layers have a potential alteration state through the later volcanic activities that extended up to 2.5 Ma (Aydar et al. 2012). In this context, this study aimed to investigate detailed mineralogical and geochemical characteristics of altered ignimbrites and to understand the origin and occurrence of clay-rich alteration zones through hydrothermal alteration.

Geological setting and lithology

The study area in the central part of the CAVP (Fig. 1) has been investigated throughout the last few decades in terms of its volcanology context (Aydar et al. 2012 and references therein). The CAVP as a plateau with an altitude of 1400–1500 m is dated as Miocene to Upper Holocene in age. The CAVP has been reported to have a few Quaternary stratovolcanoes (Erciyes Mountain and Hasan Mountain) and numerous monogenetic outlets (cinder cones, maars, domes) (Aydar and Gourgaud 1998).

Miocene volcanic complexes and lava flows are also associated with ignimbrites (e.g., Aydar and Gourgaud 1998; Aydar et al. 2012). This unit is underlain by sedimentary, magmatic, and metamorphic basement rocks (Fig. 1). The region has a topographical slope in the north direction, bounded by the Taurus Mountains in the south, and two distinct Quaternary stratovolcanoes; Hasan Mountain and Erciyes Mountain, respectively in the west and east. Miocene-Pliocene ignimbrites cover a total area of 20,000 km^2 (Le Pennec et al. 1994; Aydar et al. 2012).

Large pyroclastic discharge deposits were formed by covering the surface with high-intensity pyroclastic currents caused by the explosion of magmas ranging from volcanic rocks with composition of dacites to rhyolites (Smith 1960; Wilson et al. 1980; Aydar et al. 2012). The pyroclastic layers are distributed as very common and distinct deposits and these discharge deposits may have individually traveled long distances (e.g., Wilson et al. 1995; Aydar et al. 2012). The nomenclature of ignimbrite was taken from Le Pennec et al. (1994), in which 10 ignimbrite members of Ürgüp Formation were identified from old to young: Kavak, Zelve, Sarımadentepe, Sofular, Cemilköy, Tahar, Gördeles, Kızılkaya, Valibabatepe, and Kumtepe. They are separated by abundant rhyolitic-dacitic ignimbrites, lacustrine deposits, earth, or lava flows (Pasquaré 1968). This study covers the Upper Miocene Kavak ignimbrite member, which is dated as the oldest ignimbrite unit in the stratigraphic sequence (Aydar et al. 2012). However, the Kavak ignimbrite was previously defined as the upper and lower Göreme ignimbrite (Schumacher et al. 1990; Ercan et al. 1994), but the Kavak ignimbrite term is preferred in recent studies (e.g., Aydar et al. 2012 and references therein). Considering the stratigraphic position of the Kavak ignimbrite and K/Ar dating data, Upper Miocene age is preferred. In the K/Ar analysis of biotite minerals of the Kavak ignimbrite, the following ages were obtained by previous researchers: 8.6 ± 1.7 Ma (Innocenti et al. 1975); 11.2 ± 2.5 Ma (Temel 1992), and 8.96 ± 0.2 Ma (Schumacher et al. 1990). The mean age was determined by these researchers and in recent studies an age of 9.12 ± 0.09 Ma was reported (Aydar et al. 2012).

Field observations show that ignimbrites have lapilli structures and parts resembling karstic gaps are observed in some parts of the white-gray altered unit (Fig. 2). The upper parts of the Kavak ignimbrite unit exhibits fine-grained stratified facies at lower parts and massive ignimbrite facies at uppermost parts (e.g., Guzmán et al. 2020) (Fig. 2a–c). The erosional differences related to silica-rich (slightly-eroded) in massive ignimbrite facies and clay-rich (highly-eroded) levels of fine-grained stratified parts show a similar appearance to fairy chimneys (Fig. 2a, b). Highly altered clay-rich (argillized) ignimbrite layers mostly exhibit clean white colors (Fig. 2b, c). Iron oxy-hydroxide (hematite, goethite/limonite) zones within the altered ignimbrite layers display orange-yellow colors due to the effect of hydrothermal fluids circulation especially throughout the fault planes and fractures (Fig. 2d, e).

Materials and methods

A total of 30 samples were collected from different levels and locations between Nevşehir and Avanos (Fig. 1) and analyzed by several methods: optical microscopy (OM), scanning electron microscopy with energy dispersive X-ray spectroscopy (SEM-EDX), X-ray fluorescence spectroscopy (XRF), and inductively coupled plasma mass spectrometry (ICP-MS) methods. The X-ray diffraction (XRD), XRF, SEM-EDS, and ICP-Ms analyses were conducted at the Central Research Laboratory of Niğde Ömer Halisdemir University, Turkey. XRD analyses of some samples were performed at the Geology Department of the University of Cincinnati, USA. The oxygen and hydrogen isotope analyses were performed at the Stable Isotope Laboratory of Cornell University, USA.

OM studies were conducted by Olympus binocular transmitted light microscopy to determine textural and mineralogical features of altered ignimbrites.

XRD analysis was performed using a Panalytical EMPYREAN Advance Diffractometer for determining the whole rock and clay fraction mineral composition. The analysis were made by using CuKα (λ = 1.541871 Å) radiation. Diffraction patterns were recorded from 5 to 70° 2θ with a scan rate of $3°min^{-1}$ for whole-rock, 5 to 30° 2 θ with a scan rate of $2°min^{-1}$ for clay fraction. Samples for clay analysis (< 2 μm) were prepared by separation of the clay fraction by sedimentation, followed by centrifugation of the suspension, after overnight dispersion in distilled water. The clay particles

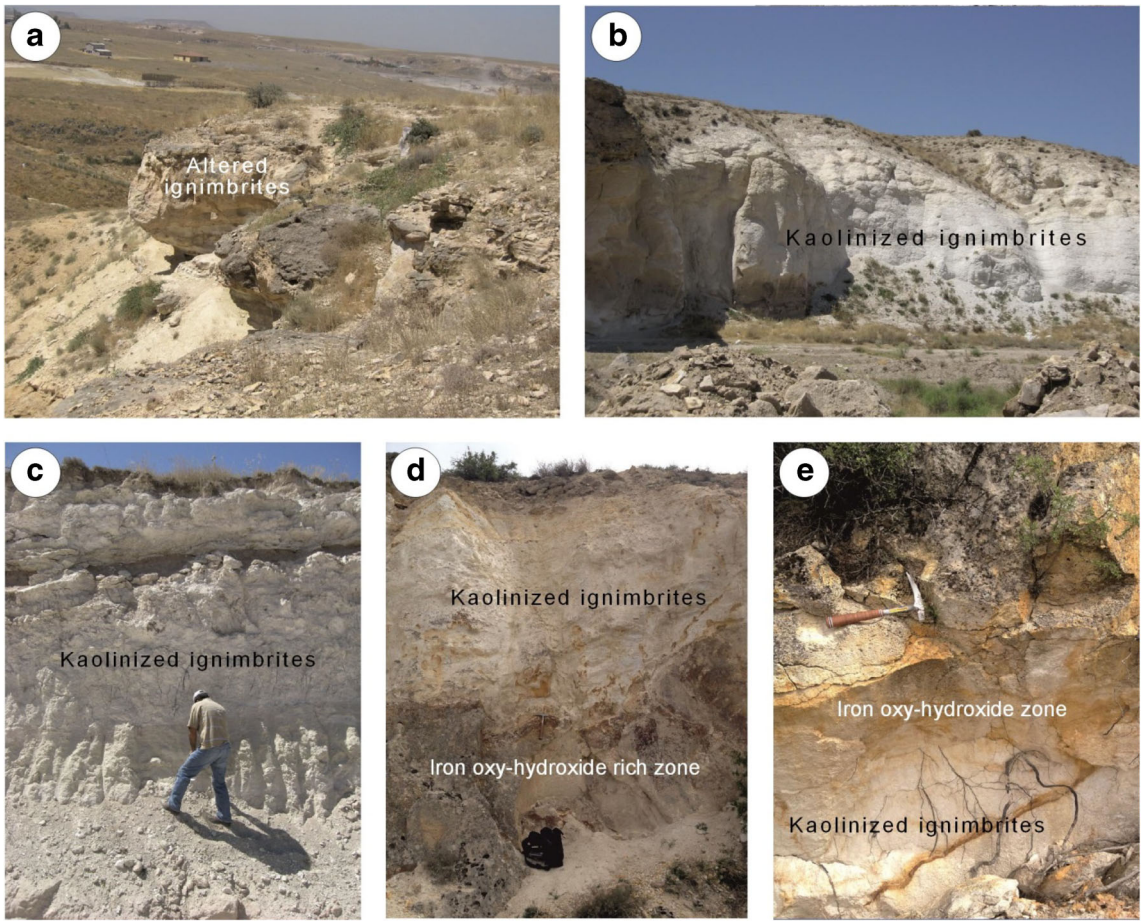

Fig. 2 Field observations of the Kavak ignimbrite unit. **a** Erosional differences for altered ignimbrite layers related to silica-rich (slightly-eroded) and clay-rich (highly-eroded) levels known as fairy chimneys. **b**, **c** Highly altered (argillized) ignimbrite layers. **d**, **e** Iron oxy-hydroxide (hematite, goethite/limonite) zones along the cracks and/or fault zones within the altered ignimbrite layers

were dispersed by ultrasonic vibration for about 15 min. Three oriented clay specimens were prepared from each sample by the following protocol: air dried, ethylene-glycol-solvated at 60 °C for 2 h, and thermally treated at 550 °C for 2 h, respectively. Rietveld optimization for XRD data was performed with PanAlytical software X'Pert Highscore Plus.

SEM–EDX analysis was performed in a Zeiss EVO 40XVP instrument. Representative clay-rich samples were prepared for SEM–EDX analysis by gluing the fresh, broken surface of the sample onto an aluminum sample holder that had been covered with double-sided tape and coated with a thin film (~ 350 Å) of gold, using a Giko ion coater.

pH values of the hydrothermally altered samples were determined from homogenized powder samples within the distilled water (suspension) by using a pH meter (Isolab/pH-Orp). Fourier-transform infrared spectroscopy (FTIR) analyses were achieved from Bruker Vertex 70 Brand instruments.

The major oxide chemical analyses were obtained for twenty-one representative pure or nearly pure kaolin samples by XRF (Philips Panalytical Zetium). Chemical analyses were performed using the rock standards supplied by MBH Reference Materials and Breitlander companies. The accuracy for elements was ± 2%. Loss on ignition (LOI) of each sample was also determined by drying the samples at 105 °C overnight, followed by calculation of their H_2O content and other volatiles at 1050 °C. Trace element analyses were acquired by inductively couple plasma-mass spectroscopy (ICP-MS). The detection limits ranged from 0.1 to 5 ppm.

The stable isotope analyses were conducted in a Thermo Delta V isotope ratio mass spectrometer (IRMS) interfaced to a temperature conversion elemental analyzer (TC/EA). The results were given as $\delta^{18}O$ and $\delta^{2}H$ or δD standardized with Vienna Standard Mean Ocean Water (V-SMOW). Delta values are measured in units of per mil (‰). Precision is ability of the instrument to consistently measure the same value for a known sample throughout the course of the analytic run. The standard deviation for the internal standard Inter Benzoic Acid for $\delta^{2}H$ is 4‰, and for $\delta^{18}O$ is 0.09‰. Corrections were performed using two-point normalization (regression) based on standards USGS 601 and USGS 602 for $\delta^{18}O$ and IAEA CH7 and EMA-P1 for $\delta^{2}H$. Detailed analytical procedures are given in the laboratory website (www.cobsil.com).

Results and discussion

Petrography results

Optical microscopy

The glassy ash tuffs of the Kavak ignimbrite unit has a porphyritic texture containing phenocrysts of plagioclase, quartz, hornblende, biotite, opaque mineral (iron oxide), and alkali feldspar within the devitrified volcanic groundmass associated with pumice grains. According to chemical compositions, ignimbrites have mostly dacite and trachyandesite, and partly rhyolite composition (Temel et al. 1998; Ertek and Öner 2008). Plagioclase phenocrysts having polysynthetic twinning show fractured and/or cracking texture indicating the pyroclastic eruption (Fig. 3a). Pyroclastic eruption also deformed the biotite phenocrysts as shown by the development of fringes along the cleavage planes (Fig. 3b). The quartz minerals exhibit primary magmatic texture which was corroded by the volcanic groundmass (Fig. 3c).

The optical microscopic observations of intensely altered ignimbritic rocks show silicification and argillization (Fig. 4). Primary magmatic quartz (Q_m) commonly corroded the glassy volcanic groundmass which was extremely devitrified to silica and clays (Fig. 4a–d). The pumice grains having porous texture were also altered to silica and clay minerals (Fig. 4a, b). Biotite phenocrysts were extremely altered to opaque (iron oxide) minerals (opacitized) and some grains were completely replaced by opaque minerals and exhibit a pseudomorphic texture (Fig. 4c, d). Glass shards are mainly observed as completely silicified grains (Qz_h), whereas clay occurrences are completely related to the volcanic glassy matrix (Fig. 4c–f). The petrographic observations indicate that the common alteration products are cryptocrystalline silica (quartz) and clay (kaolinite/dickite) minerals. Hydrothermal alteration related silica minerals were precipitated as both pore filling (euhedral spherical relicts) and replacement of glass shards (sharp edged grain), where clays were developed due to transformation from the glassy volcanic matrix.

Scanning electron microscopy

The scanning electron microscopy (SEM) investigation of argillized samples shows vermicular (vermiform) kaolinite/dickite booklets (Fig. 5a). The stacking thickness of booklets reached up to 30 μm. Kaolinite/dickite minerals exhibit irregular stacking of pseudo hexagonal kaolinite platelets, in which kaolinite and dickite minerals are distinguished by uniform and prolonged shape of plates (Fig. 5b). Fine-grained euhedral alunite crystals (approximately 1 μm in size) are also associated with the kaolinite/dickite minerals (Fig. 5c). The thicknesses of the individual kaolinite/dickite plates smaller than 1 μm (~ 200 nm), and horizontal and/or lateral diameters of pseudo-hexagonal plates are around 2 μm (Fig. 5d). The vermicular packing of kaolinite/dickite plates exhibits sequential (or serrated) stacking.

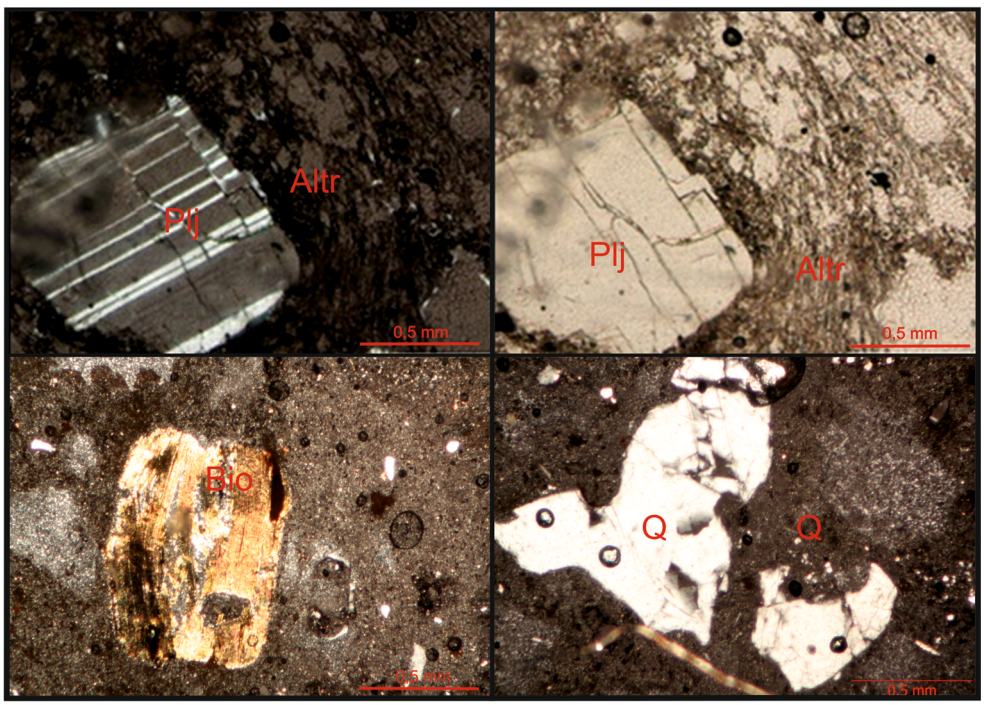

Fig. 3 Optical microscope images of ignimbrites. **a**, **b** Fractured plagioclase phenocryst within the devitrified (altered) volcanic groundmass and pumice (**a**: crossed nicols, **b**: open nicol). **c** Deformed biotite phenocryst with fringe texture along the cleavage planes within the siliceous volcanic groundmass (Crossed nicols). **d** Corroded quartz phenocrysts within the siliceous volcanic groundmass (crossed nicols)

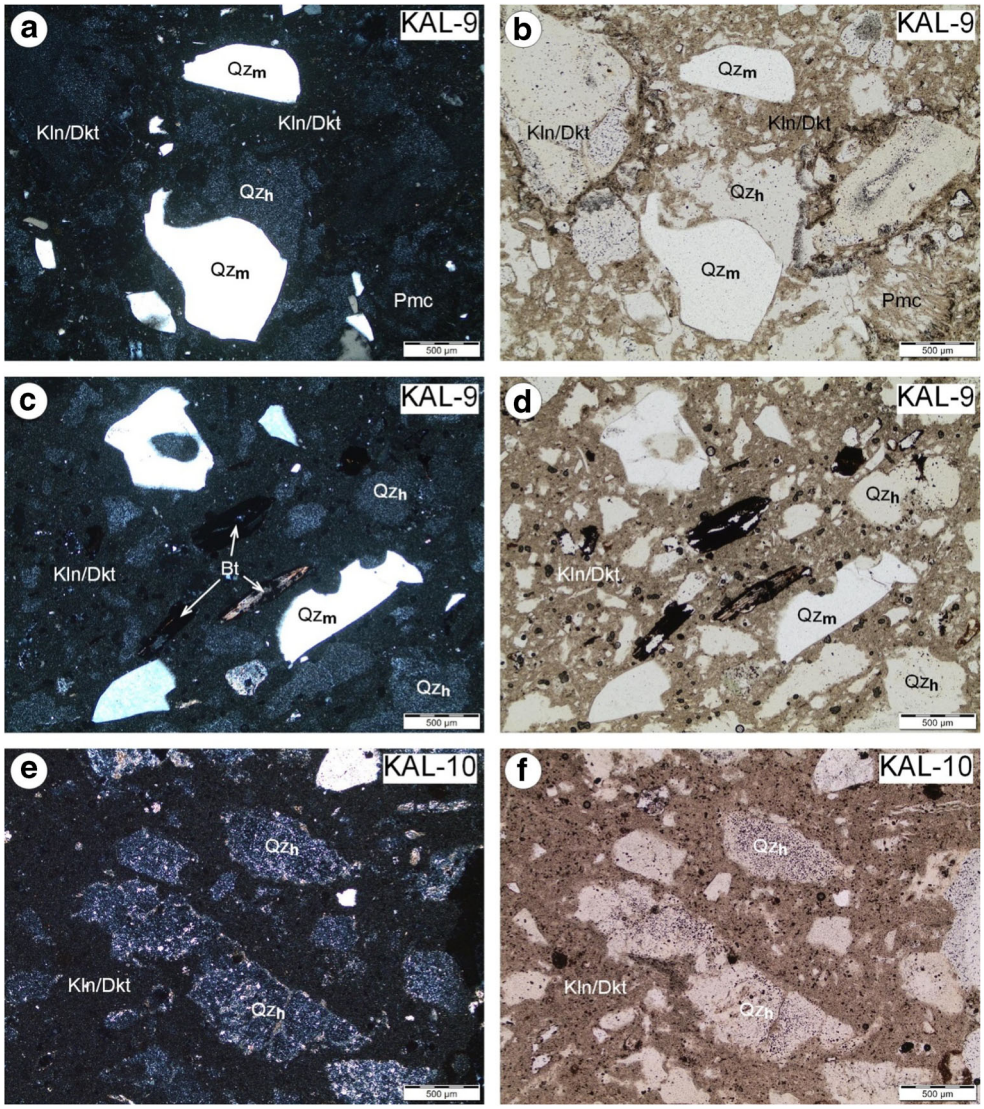

Fig. 4 Optical microscope images of altered ignimbrites. **a**, **b** Quartz phenocrysts (primary magmatic quartz-Q_m) corroded by silicified (hydrothermal quartz-Q_h) and argillized (kaolinite/dickite-Kln/Dkt) volcanic groundmass (glassy ash), and microporous pumice fragments (**a**: Crossed nicols, **b**: Open nicol). **c**, **d** Corroded quartz and opacitized biotite phenocrsyts associated with the argillized volcanic groundmass (**c**: Crossed nicols, **d**: Open nicol). **e**, **f** Silicified glass shards and pore-filled fine-grained hydrothermal quartz and argillized volcanic groundmass (**e**: crossed nicols, **f**: open nicol)

Mineralogy results

X-ray diffraction

The altered ignimbrite samples are divided into three groups, as slightly, moderately, and highly altered, with respect to their alteration grades on the basis of their mesoscopical (plasticity related to argillization), petrographical (primary magmatic vs. alteration related components), mineralogical (clay content), and chemical (loss on ignition values related to clay content) properties. X-ray diffraction (XRD) analyses of the samples having different alteration grades collected from several profiles and/or layers are given in Table 1.

The samples contain mainly quartz and clay, and minor amounts of alunite and jarosite. The clay fraction is composed of kaolinite and dickite and rarely illite and mixed-layered illite/smectite (I-S) (Fig. 6). The absence of feldspar minerals seems to be related to their being completely transformed to clays during hydrothermal alteration. Subordinate amounts of illite (or mica) and I-S could be associated with the magmatic mica relicts (see Fig. 4c, d) and their transformation product from mica though I-S to finally smectite.

The kaolinite and dickite minerals are characterized by two reflections at 7.15 and 3.57 Å in the range of 2θ = 2–30° (Fig. 6). The kaolinite and dickite peaks are not affected by ethylene glycol treatments but collapsed upon heating to 550 °C (e.g., Moore and Reynolds 1989). The highly altered ignimbrites have somewhat higher clay (kaolinite and dickite), alunite, and jarosite contents than moderately and slightly altered ones (Table 1, Fig. 7). The diagnostic peaks for both kaolinite and dickite minerals were used for distinguishing peaks for both minerals from unoriented powder patterns as previously preferred by Bailey (1980, 1988) (Fig. 7). The representative diagnostic peaks of

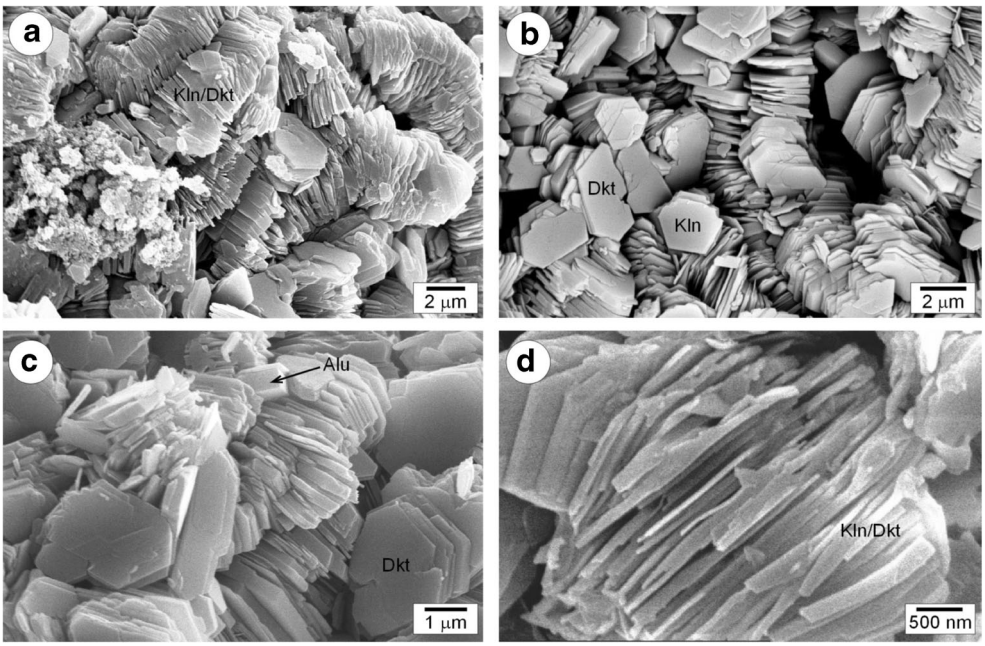

Fig. 5. SEM photomicrographs of kaolinite/dickites. **a** Vermicular (vermiform) euhedral kaolinite/dickite booklets. **b** Tightly irregularly stacked kaolinite/dickite booklets, pseudohexagonal plates of kaolinites and dickites exhibit uniform and prolonged shapes, respectively. **c** Euhedral alunite crystals and prolonged dickites. **d** Tightly packed kaolinite/dickite booklets

kaolinite and dickite minerals are clearly distinguished from schematic X-ray powder diffraction diagrams (Brown and Brindley 1980; p. 330; Fig. 5.2) in the 2θ ranges of 19–27° and 34–42° (Fig. 7).

Table 1 Mineralogical composition of bulk and clay-size fraction (< 2 μm) of the samples

Sample No	Bulk					Clay fraction		
	Qz	Cal	Alu	Jrs	Clay	Kln	Dkt	Ilt/I-S
Slightly altered								
KAL-1	62				38	68	32	
KAL-2A	38		±		62	65	35	
KAL-2B	37		±		63	71	29	
KAL-3	70			±	30	78	20	2
KAL-9	55				43	58	40	2
KAL-10	47				53	47	53	
KAL-11	74				26	62	38	
Moderately altered								
KAL-1C	22		±		78	49	51	
KAL-2	46				54	92	6	2
KAL-12A	66	2			33	39	61	
KAL-12B	49				51	57	43	
Highly altered								
KAL-1A	48		±		52	90	10	
KAL-1B	10			±	90	60	40	
KAL-3A	8			±	92	55	45	
KAL-3B	18				82	60	40	
KAL-3C	39		±		61	77	23	
KAL-4A	28			±	72	53	46	1

+: 20%, ±: trace (< 5%). *Qz* quartz, *Cal* calcite, *Alu*: alunite, *Jrs* jarosite, *Kln* kaolinite, *Dkt* dickite, *Ilt* illite, *I-S* mixed-layered illite-smectite

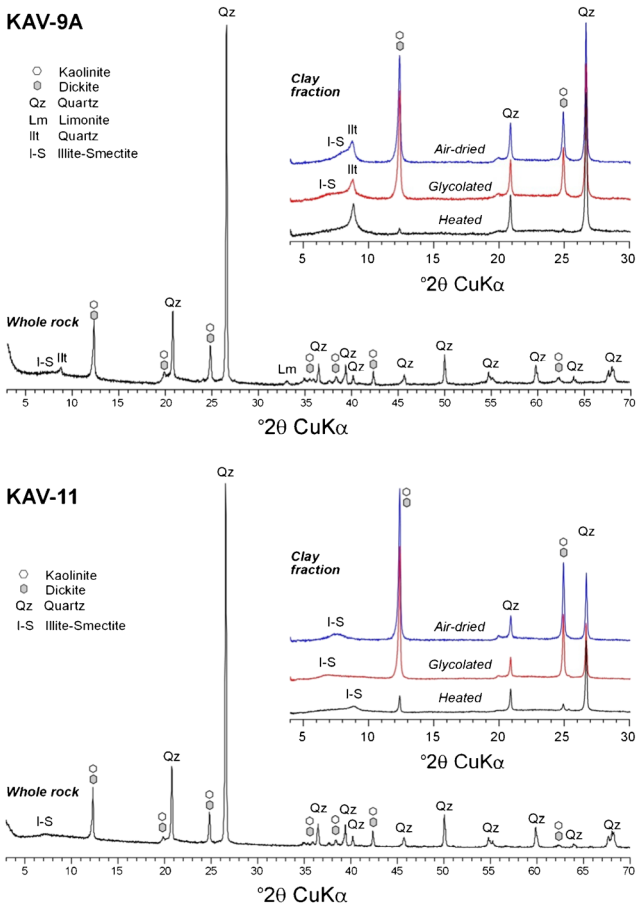

Fig. 6 Whole rock and clay fraction of altered ignimbrite sample

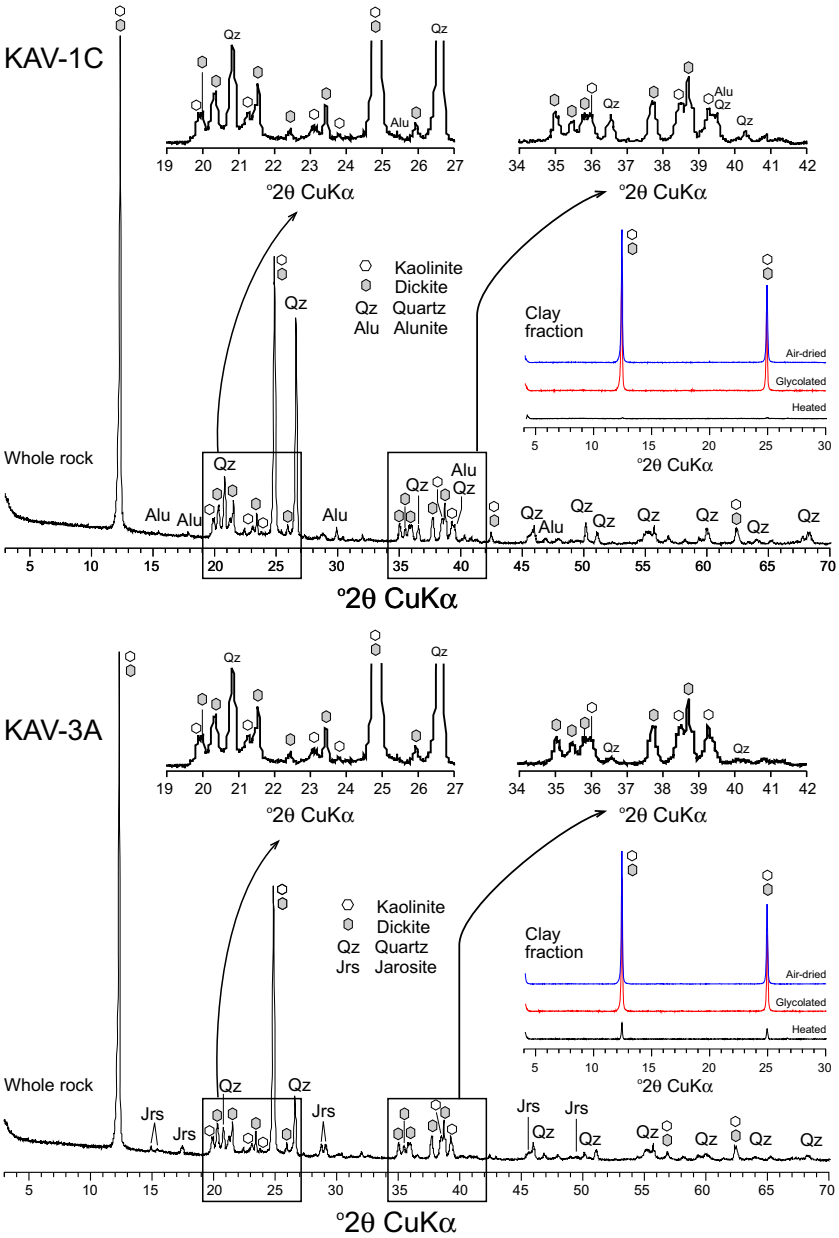

Fig. 7 Representative XRD patterns of whole rock and clay fraction of altered ignimbrite samples. Diagnostic peaks used for distinguishing kaolinite and dickite minerals are taken from Bailey (1980, 1988)

Fourier-transform infrared spectrometer

The Fourier-transform infrared spectroscopy (FTIR) properties of altered ignimbrite samples indicate sharp stretching OH regression bands typical for both kaolinite and dickite at 3689, − 3670, − 3662, and 3620 cm^{-1} (Fig. 8). The 3620 cm^{-1} band belongs to the internal stresses of the -OH groups between the layers of kaolinite structure. The 1005–1030 cm^{-1} bands observed in the fingerprint region belong to the Si-O stresses at the center of the kaolinite/dickite crystals. The band of the hydroxyl group on the inner surface of the kaolinite/dickite is 911 cm^{-1}. The weak bands at 745 and 700 cm^{-1} in the spectra are probably related to the perpendicular Si-O vibrations of the surface hydroxyl layer. The bands around 3000 cm^{-1} are thought to indicate the presence of alunite (Fig. 8).

Geochemistry results

Major element geochemistry

The major element compositions of altered ignimbrite samples are given in Table 2 and Fig. 9. According to loss on ignition values, three alteration groups are divided as slightly altered (5.00–7.76 wt.%), moderately altered (8.00–8.36 wt.%), and highly altered (10.90–13.08 wt.%) ignimbrites. In order to understand the chemical differences related to alteration, major element concentrations of altered ignimbrites are compared with the non-altered ignimbrite composition (Temel et al. 1998). The major oxide compositions of the altered ignimbrite samples exhibit a similar trend, but some differences with respect to the non-altered sample

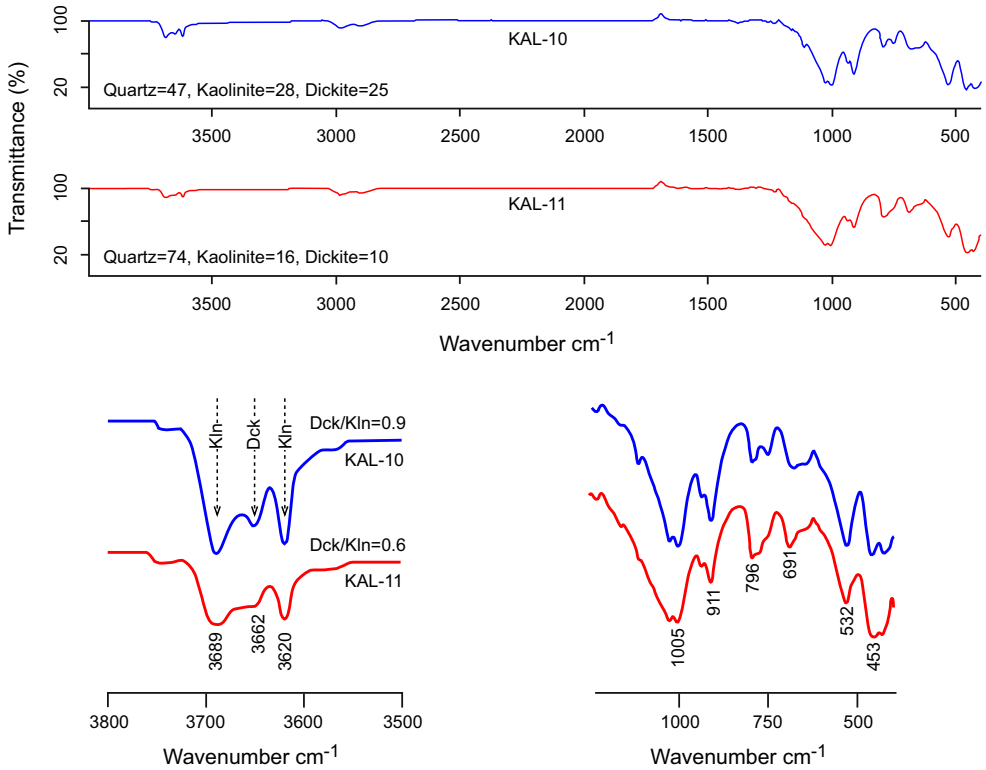

Fig. 8 FTIR spectra of altered ignimbrite samples

(Fig. 10). The mean values of TiO_2, Al_2O_3, and P_2O_5 increase, whereas SiO_2, MnO, MgO, CaO, Na_2O, and K_2O decrease in the altered samples (Table 2, Fig. 9). The enrichment in Al_2O_3 is resulting from hydrothermal alteration, i.e., kaolinization. From slightly altered to highly altered ignimbrites and finally to theoretical pure kaolinite, SiO_2 slightly decreases but Al_2O_3 and LOI distinctly increase together with the increasing degree of alteration (Fig. 10). The unclear decreasing of the SiO_2 contents may be caused by the cryptocrystalline quartz occurrences together with clays. Kaolinite/dickite-rich clay fractions in highly altered ignimbrite samples have excess Si and Fe because of the presence of cryptocrystalline quartz and goethite in the clay fraction, respectively; therefore, their structural formulas did not calculate because of the charge imbalance.

Trace-element and REE compositions

The trace element concentrations of altered ignimbrites are given in Table 2. Some trace element compositions are evaluated on the chondrite-normalized multiple trace element and REE spider diagram (Fig. 11a, b). All elements, except for Rb, Sr, and P, show obvious enrichments. Rb, Ba, and Sr show a broad range, i.e., decreased 0.3 times and enriched up to c. 9400 times, with respect to chondrite (Fig. 11a). However, the contents of trace elements of altered ignimbrites exhibit similar trends with host-rock composition; there are some differences for different grades of alterations with respect to the non-altered host-rock. Chondrite-normalized (Sun and Mc Donough 1989) Rb, K, and Yb average contents are noticeably lower than ignimbrite host-rock (Fig. 11b), indicating element mobility during acidic hydrothermal alteration. Contrary to this, La, Ce, Nd, Sm, and Ti are enriched in altered ignimbrites, which seem to be related to increasing the hydrothermal clay content. In addition to this, some elements (Ba, Sr, Eu, Ti, Yb) show gradual increase together with the alteration degrees. In other words, the concentrations of Ba, Sr, and Eu increase, but Ti and Yb decrease together with the increasing alteration degree (Fig. 11b).

The chondrite-normalized REE values of altered ignimbrites have a similar trend with the non-altered ignimbrite sample but exhibit a wide range spider diagrams associated with the different degrees of alteration (Fig. 12a). All of the altered ignimbrites as well as the host-rock exhibit clear enrichment of REE with respect to the chondrite. The REE spider diagram of altered ignimbrites shows a distinct decreasing trend from La to Gd (light rare earth elements, LREE) and a rather stable distribution from Dy to Lu (heavy rare earth elements, HREE) without any negative Eu anomaly (Fig. 12b). The altered ignimbrites have enrichment for LREE but depletion for HREE, when compared to the non-altered ignimbrite host-rock. The highly altered samples have lower REE values than those of slightly and moderately altered ignimbrites, except for Eu, Gd, and Er.

Table 2 Major (wt %) and trace (ppm) element composition of the altered ignimbrites

	Slightly-altered							Moderately-altered				Highly-altered						Host-rock
	KAL-1	KAL-2A	KAL-2B	KAL 3	KAL 9	KAL 10	KAL 11	KAL-1C	KAL 2	KAL 12A	KAL 12B	KAL-1A	KAL-1B	KAL-3A	KAL-3B	KAL 3C	KAL 4A	U-349
SiO_2	73.87	62.52	69.84	73.34	67.18	75.94	80.77	67.42	71.39	71.67	68.00	63.67	55.41	46.52	51.47	60.65	56.86	72.34
TiO_2	0.16	0.17	0.29	0.25	0.39	0.20	0.15	0.26	0.30	0.23	0.25	0.13	0.28	0.12	0.24	0.14	0.31	0.15
Al_2O_3	17.30	28.10	26.92	13.35	18.01	16.79	15.01	22.11	18.32	15.58	20.14	21.59	31.30	36.19	32.83	25.42	27.94	13.52
Fe_2O_3	0.18	0.61	0.72	2.66	3.67	1.38	0.14	1.78	0.60	2.54	1.80	2.07	0.82	2.63	0.71	0.27	1.25	1.33
MnO	0.002	0.002	0.002	0.002	0.002	0.007	0.006	0.011	0.002	0.017	0.002	0.002	0.005	0.002	0.002	0.002	0.002	0.060
MgO	0.17	0.06	0.09	0.33	0.48	0.00	0.03	0.00	0.35	0.17	0.13	0.48	0.10	0.24	0.12	0.00	0.12	0.25
CaO	0.06	0.04	0.05	0.07	0.16	0.12	0.10	0.11	0.16	1.66	0.08	0.05	0.09	0.07	0.02	0.08	0.10	1.91
Na_2O	0.18	0.07	0.00	0.00	0.05	0.00	0.00	0.01	0.11	0.00	0.00	0.12	0.25	0.11	0.00	0.00	0.06	2.07
K_2O	0.28	0.23	0.35	0.99	1.12	0.16	0.27	0.37	0.80	0.42	0.42	0.37	0.13	0.36	0.11	0.36	0.56	4.2C6
P_2O_5	0.097	0.059	0.078	0.058	0.041	0.025	0.013	0.178	0.043	0.058	0.058	0.118	0.044	0.236	0.024	0.141	0.115	0.050
LOI	6.50	7.76	7.43	7.14	7.50	6.20	5.00	8.14	8.00	8.36	8.36	10.90	12.00	13.00	13.08	12.50	11.88	4.30
Total	98.79	99.61	105.75	98.18	98.59	100.81	101.48	100.38	100.07	100.70	99.23	99.50	100.41	99.47	98.62	99.56	99.18	100.24
Cr	1.27	0.79	2.15	21.76	1.05	1.00	1.00	3.75	6.48	1.15	52.07	3.16	4.85	29.27	50.56	33.28	1.00	24.90
Ni	0.14	0.08	0.27	10.60	0.98	0.05	0.05	0.13	0.86	0.48	15.23	3.43	− 0.09	6.11	17.99	18.65	0.05	4.70
Co	0.56	3.72	2.52	6.22	2.44	3.43	0.31	0.62	0.09	4.02	54.35	0.73	− 0.63	0.09	41.64	2.42	0.05	0.60
V	16.58	14.11	20.12	178.16	9.99	6.34	0.98	40.95	21.31	24.39	278.97	24.38	53.01	256.94	283.38	169.79	2.15	6.20
Cu	3.76	4.17	3.79	49.27	2.54	1.00	1.00	19.04	3.48	2.84	69.02	6.99	7.09	76.37	58.33	38.90	1.00	n.a.
Zn	0.08	0.08	0.08	10.96	0.08	0.08	0.08	0.08	0.99	0.10	13.80	0.65	0.08	3.48	9.20	8.08	0.08	n.a.
As	1.68	2.55	3.81	9.52	0.50	6.69	0.50	54.00	0.56	0.50	5.22	46.78	40.00	91.02	165.53	15.81	1.49	n.a.
Sb	9925.07	11237.55	6974.03	66370.34	5732.64	29693.54	1052.63	637280.00	5551.60	7951.41	163630.00	155620.00	228750.00	1269800.00	722180.00	83181.81	1303.80	n.a.
Ge	460.71	690.34	835.65	11476.20	1098.07	560.21	26.40	1855.49	1114.94	2124.58	15992.41	2017.44	1584.58	10987.34	9005.08	4188.76	166.06	n.a.
Be	0.05	0.05	0.05	0.12	0.05	0.05	0.05	0.05	0.05	0.05	1.43	0.05	0.05	0.07	0.13	0.03	0.05	n.a.
Rb	3.06	3.34	4.72	152.67	17.99	1.60	0.83	2.39	33.65	14.08	126.32	2.53	2.12	57.66	72.84	29.20	2.00	171.60
Ba	632.76	369.18	196.71	2604.93	54.98	20.15	5.97	492.70	564.19	163.92	237.94	191.58	694.40	18886.60	22592.53	5318.30	115.46	948.80
Sr	132.52	29.59	32.70	970.71	32.91	6.15	2.14	211.09	138.89	50.70	997.82	185.52	103.58	4310.89	1051.89	1056.56	9.19	240.60
Ga	10.00	6.73	10.48	57.84	3.10	2.00	0.03	14.87	12.13	6.33	230.50	9.98	22.76	93.82	124.82	85.34	0.85	12.30
U	0.01	0.01	0.01	0.01	0.01	0.01	0.01	0.01	0.03	0.01	0.01	0.04	0.09	0.11	0.23	0.01	0.01	n.a.
La	52.756	33.402	45.900	51.317	75.311	50.307	29.688	64.097	65.973	74.368	64.766	21.599	34.468	71.764	18.695	33.597	60.615	30.650
Ce	97.157	55.526	71.050	86.623	131.171	85.012	50.406	113.654	118.335	127.562	108.847	44.578	62.405	161.245	32.286	64.076	106.477	49.490
Pr	8.583	4.427	5.651	7.854	11.664	7.738	4.289	8.849	10.371	11.001	9.009	4.758	5.162	12.790	3.112	5.769	9.172	4.000
Nd	25.160	10.946	13.966	22.311	35.321	22.098	11.489	26.420	31.679	31.477	25.454	15.368	13.586	32.126	8.562	16.297	26.878	11.900
Sm	3.779	1.482	1.820	3.086	5.062	3.235	1.564	3.454	4.204	3.799	3.149	2.116	1.951	4.187	1.340	2.480	3.373	2.090
Eu	1.482	0.592	0.666	1.031	1.522	0.883	0.428	1.159	1.463	1.028	0.748	0.712	0.937	2.908	1.365	0.861	1.377	0.490
Gd	15.693	7.057	7.989	11.049	14.780	8.838	5.407	13.924	15.528	13.972	9.516	6.370	9.881	33.110	14.155	8.263	15.917	0.650
Dy	1.221	0.774	0.920	1.440	2.637	2.151	1.201	1.512	1.690	1.930	1.471	0.862	1.011	2.115	1.178	0.690	1.312	1.530
Ho	0.220	0.143	0.172	0.268	0.442	0.425	0.245	0.285	0.304	0.386	0.251	0.164	0.173	0.368	0.259	0.121	0.212	n.a.
Er	23.024	10.505	13.716	16.260	35.661	23.868	11.288	20.013	26.180	31.912	19.872	16.217	13.945	32.561	8.541	15.514	26.388	1.200
Tm	0.099	0.067	0.086	0.124	0.165	0.193	0.139	0.134	0.126	0.159	0.098	0.064	0.070	0.157	0.144	0.039	0.073	n.a.
Yb	0.749	0.594	0.747	1.021	1.187	1.497	1.216	1.145	1.022	1.207	0.779	0.513	0.567	1.311	1.213	0.360	0.573	1.380
Lu	0.173	0.080	0.101	0.136	0.140	0.201	0.176	0.163	0.133	0.142	0.083	0.098	0.098	0.183	0.180	0.038	0.056	0.220

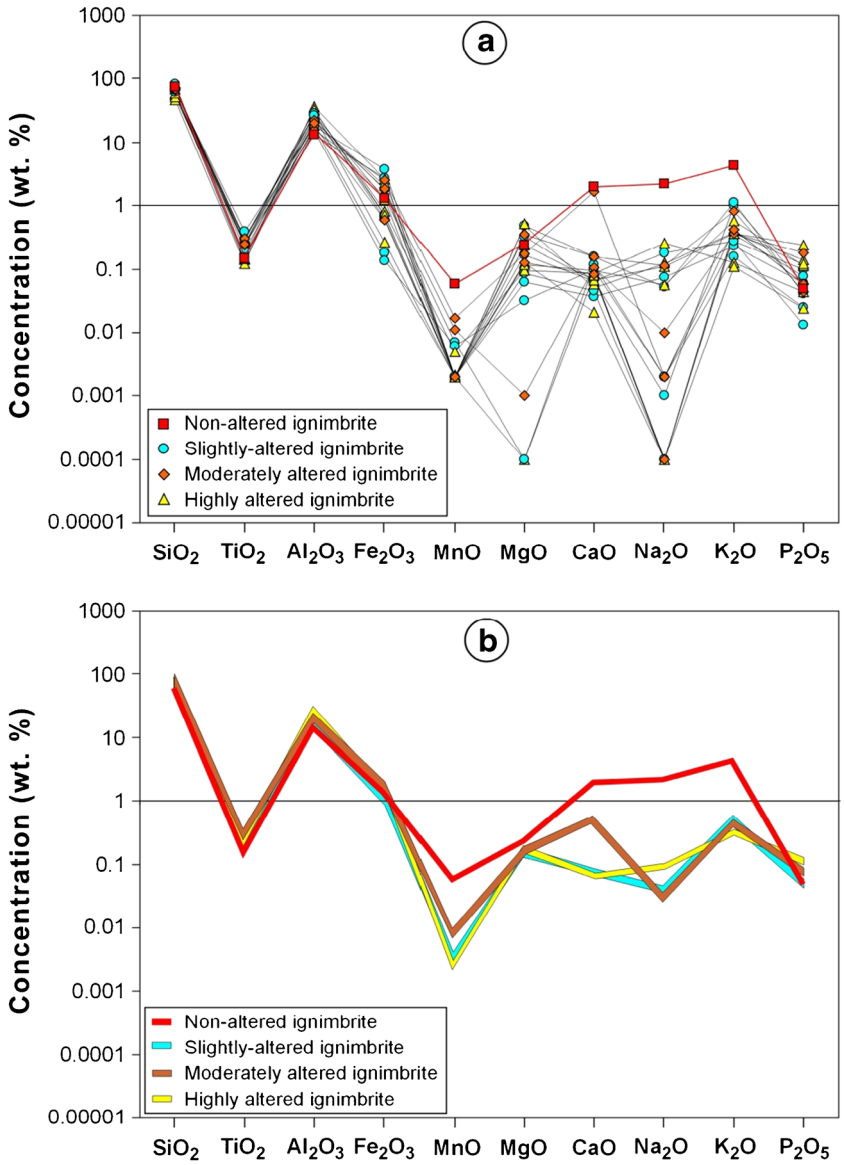

Fig. 9 Major oxide (wt. %) concentrations of kaolinites/dickites from ignimbrite samples having different stage of alteration. Fresh (non-altered) ignimbrite composition is taken from Temel et al. (1998)

Oxygen and hydrogen isotope geochemistry

Oxygen and hydrogen isotope compositions of twelve pure or nearly pure clay-sized (< 2 μm) kaolin samples show that the $\delta^{18}O$ and δD ‰ (SMOW) values vary from 3.10 to 9.18 and from 79.97 to 94.31, respectively (Table 3). The calculated $\delta^{18}O$ and δD ‰ (SMOW) for mineral-forming water composition (assuming a temperature of 200 °C) from the equations of Sheppard and Gilg (1996) and Gilg and Sheppard (1996) are also given in Table 3. The isotope data of dickite/kaolinite samples and calculated waters are presented in a $\delta^{18}O$ vs δD ‰ binary diagram (Fig. 13a), together with the meteoric water line (Craig 1961), supergene-hypogene line (Sheppard et al. 1969), kaolinite line (Savin and Epstein 1970), and magmatic water field (Taylor 1974). Isotopic values of kaolinite/dickite fall completely in the hypogene area indicating hydrothermal conditions rather than weathering processes. The relatively higher dickite-bearing samples (i.e., dickite/(kaolinite+dickite, Dck*> 40%, Table 1) show relatively higher $\delta^{18}O$ and lower δD ‰ values than kaolinite-rich (Dck*< 40%) samples. The calculated water compositions on the basis of the assumed 200 °C temperature conditions locate the area between magmatic water field and meteoric water line, representing the mixture of magmatic and meteoric waters (Fig. 13a). The water composition of relatively higher dickite-bearing (Dck*> 40%) samples fall close to magmatic water, whereas kaolinite-rich (Dck*< 40%) samples fall relatively far from magmatic water composition. According to temperature-related kaolinite-water isotopic fractionation, possible local meteoric water composition is determined as $\delta^{18}O = -10‰$ and $\delta D = -60‰$ (SMOW). If clay-forming water was assumed to be completely magmatic water, the minimum temperature conditions of hydrothermal fluids should be around 250 °C (Fig. 13b). If clay-forming water

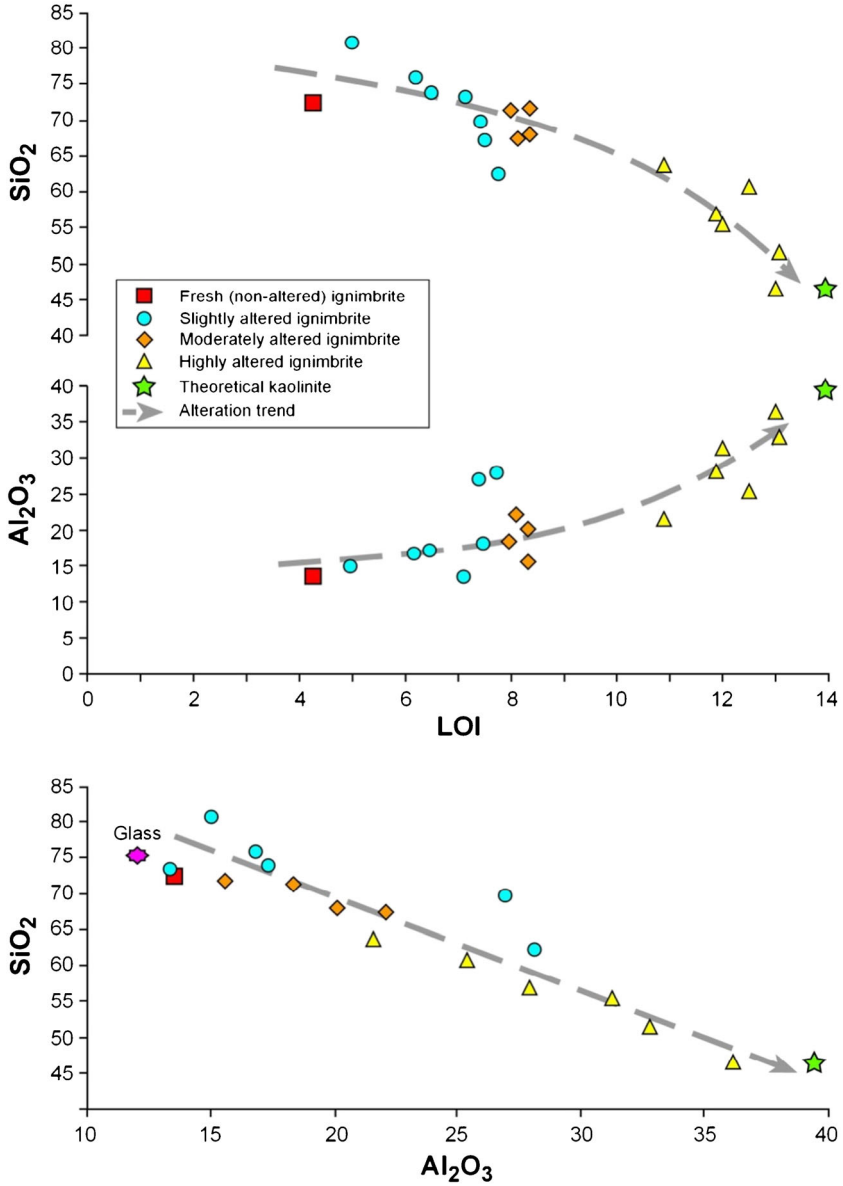

Fig. 10 Al_2O_3, SiO_2 and LOI distributions of kaolinites/dickites with regard to different alteration stages of ignimbrites. Fresh (non-altered) ignimbrite and glass composition are taken from Temel et al. (1998)

originated from meteoric waters, the maximum temperature should be around 100 °C. The presence of dickite indicates intermediate phase conditions between kaolinite and pyrophyllite which is relatively higher temperatures than those of kaolinite. Since the formation temperature of dickite should be higher than 100 °C, the clay-forming water could not have originated from entirely meteoric waters; hence, the fluids should be a mixing of meteoric and magmatic waters.

pH conditions

The measured pH values of the studied samples (Table 3) change between 4.45 and 6.60 and generally show moderately low values around pH 5. The differences in pH values for samples seem to be related to different amounts of kaolin group minerals, i.e., associated minerals such as quartz and illite.

Discussion

Hydrothermal clay occurrences

The hydrothermally altered tuff lithologies of the Kavak ignimbrite unit have mainly preserved primary porphyry texture, that indicate the in-situ alteration in a temperature dominant (steam-heated) environment. The Kavak ignimbrite unit is the oldest and lowermost level of the Ürgüp formation (Fig. 1), therefore following the deposition of the Kavak ignimbrite unit (~ 9 Ma, Aydar et al. 2012) the volcanic activity continued to the Quaternary (Temel 1992) with duration of ~ 6

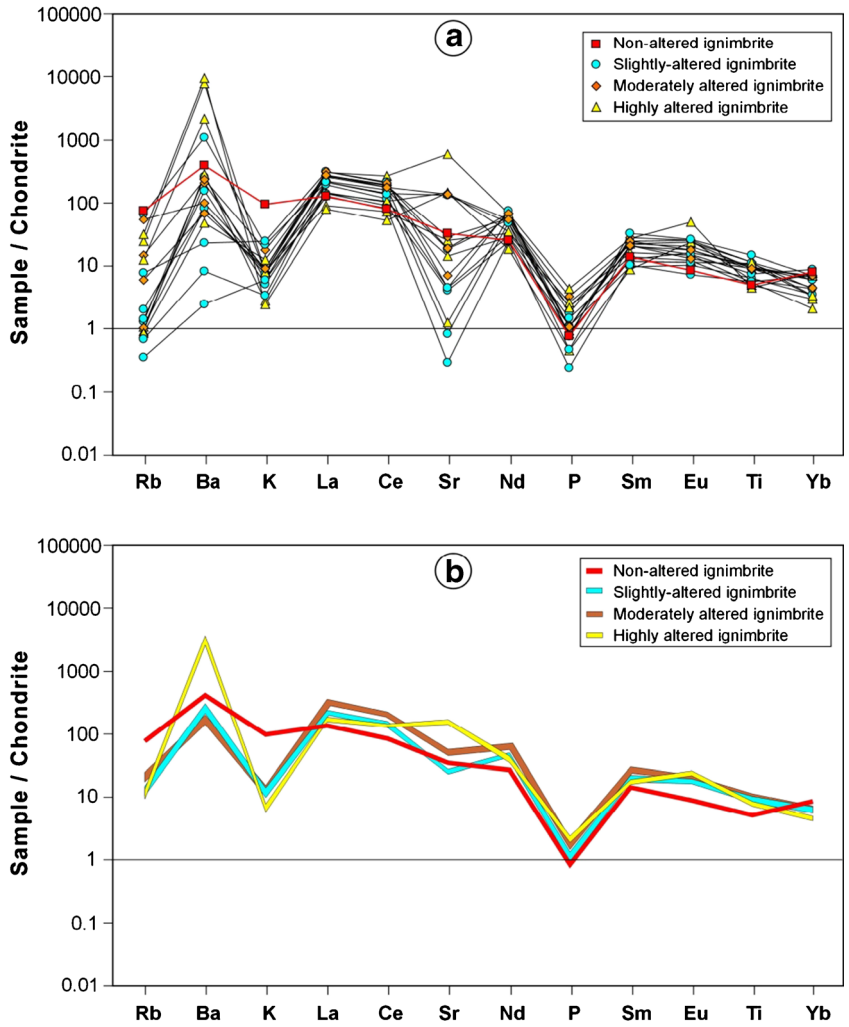

Fig. 11 Chondrite-normalized multiple trace element diagram of altered ignimbrite samples. **a** All samples. **b** Average values for different alteration degrees. Fresh (non-altered) ignimbrite composition is taken from Temel et al. (1998)

Ma, at least. Hydrothermal alteration of quartz and clay (kaolinite and dickite) occurred. Fine-grained (cryptocrystalline) quartz was developed within the pores in the groundmass and replaced by glass shards, as well. The kaolinite/dickite and association with alunite indicate the volcanism-related steam-heated surficial environments (Reyes 1990; Hedenquist et al. 2000; Simón et al. 2005; Ece et al. 2013; Ercan 2016; Mayer et al. 2016). Alunite minerals are formed as alteration products of Al-bearing minerals in relatively oxidizing, acid-sulfate conditions in the advanced argillic alteration zone (Hemely 1959; Knight 1977; Scott 1990). Its occurrences under surficial environments indicates the presence of acid sulfate fluids from H_2S gas, which evolved from a boiling hydrothermal system at depth (Reyes 1990). The very fine-grained pseudo cubic alunite crystals (Fig. 5c) seem to be related to acidic steam-heated waters.

According to petrographical observations, volcanic groundmass and volcanic glass shards as well as pumice grains completely devitrified and transformed to silica and kaolin minerals. This process could be explained as volcanic glass + water → hydrous Al-silicate gel → kaolinite/dickite reaction that is similar to those of tonsteins (Bohor and Triplehorn 1993; Spears 2012) as well as volcanic-hosted kaolin occurrences (Murray 1988; Yalçın and Bozkaya 2003):

$$2SiO2.Al2O3 + 7H2O \rightarrow Al2(OH)6.2Si(OH)4 \rightarrow Al2Si2O2(OH)2 + 5H2O$$

Volcanic glass; Al–silicate gel; Kaolinite/dickite

The absence of feldspars in altered ignimbrites indicates that the kaolin minerals also developed from feldspars under acidic environments:

$$2(K, Na, Ca)AlSi2{-}3O8 + H2O + 2H + \rightarrow Al2(OH)6.2Si(OH)4 \rightarrow 2SiO2 + 2(K+, Na+, Ca2+)$$

Regarding the kaolinite-to-dickite transformation in sedimentary environments, the temperature at which kaolinite transforms to dickite is 80 to 200 °C (Dunoyer de Segonzac 1970; Ruiz Cruz and Reyes 1998), 120–130 (Ehrenberg et al. 1993), and 140 °C (Keller 1988). However, this transformation in the hydrothermal system

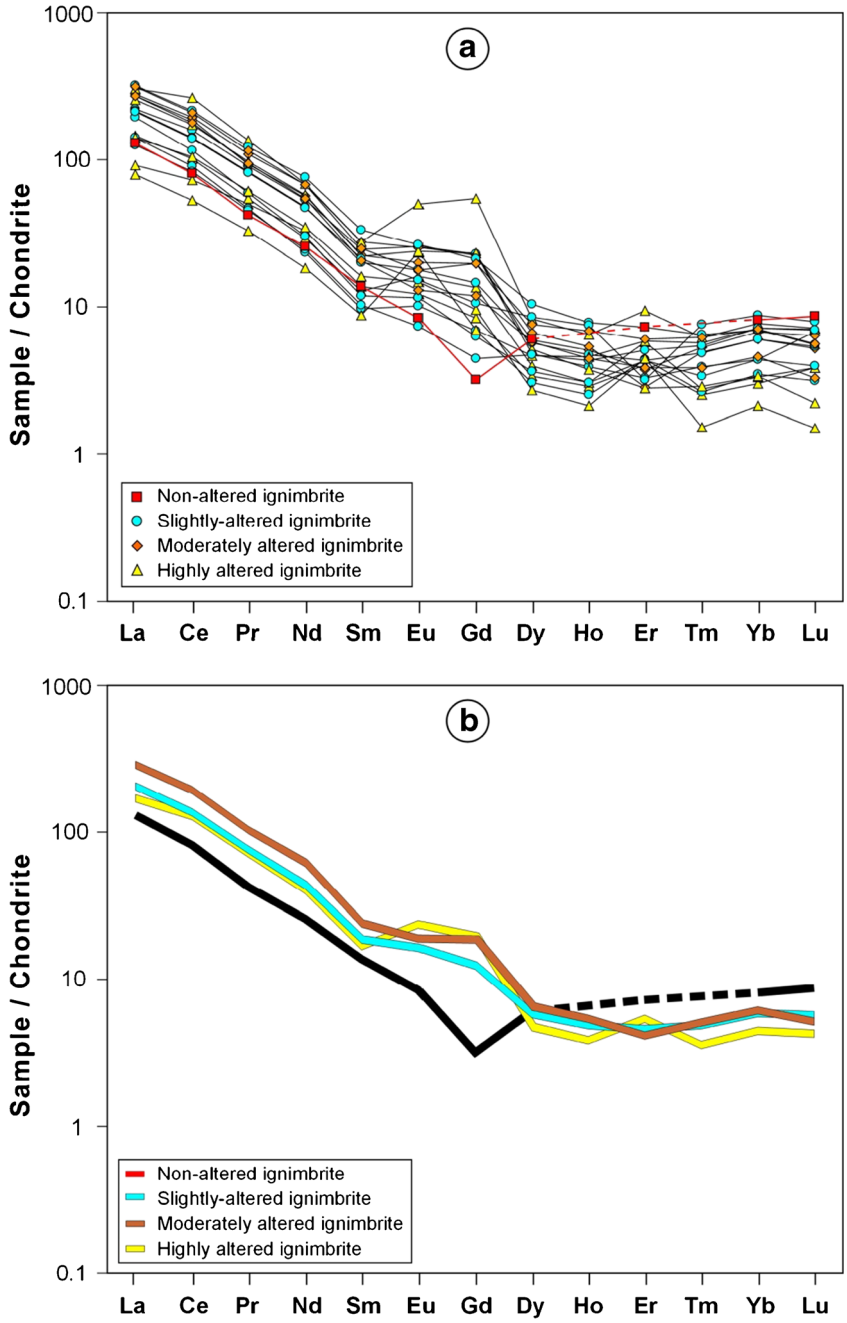

Fig. 12 Chondrite-normalized *REE* compositions of kaolinites/dickites from ignimbrite samples having different stage of alteration. Fresh (non-altered) ignimbrite composition is taken from Temel et al. (1998)

is still unknown because mixtures of dickite with kaolinite are not commonly encountered in this environment. Several studies indicate some temperature data for this transformation, i.e., the temperature of hydrothermal alteration was estimated from 150 °C (Marumo 1989) to 270–300 °C (Koh and Chang 1997; Papoulis and Tsolis-Katagas 2008). Palinkaš et al. (2009) determined 210–250 °C and 290–330 °C conditions from fluid inclusion data for kaolinite and dickite, respectively, in a metal sulfur deposit. The kaolinite-to-dickite transformation was controlled mostly by temperatures nearing the onset of hypogene conditions > 100 °C or dickite in kaolin-alunite hydrothermal deposits in Çanakkale, Turkey (Ercan et al. 2016). According to the zonation of hydrothermal kaolin group minerals with increasing temperature geothermal systems (Reyes 1990), temperature distributions were given as kaolinite (< 120 °C), dickite ± kaolinite (120–200 °C), dickite + pyrophyllite (200–250 °C), and pyrophyllite + illite (230–320 °C). Thus, dickite forms in a transitional setting between kaolinite and pyrophyllite temperature ranges. Therefore, in this study, the maximum temperature condition for kaolinite + dickite is assumed as 200 °C for estimating of the origin of hydrothermal fluids (see Fig. 13a).

Table 3 $\delta^{18}O$ and δD values of kaolinite/dickite and calculated water compositions.

Sample No	pH	$\delta^{18}O$	δD	$\delta^{18}O_{water}(*)$	$\delta D_{water}(*)$
Dck* < 40%					
KAL-1	6.60	4.33	− 82.36	− 1.27	− 64.86
KAL-1A	5.03	3.28	− 79.97	− 2.32	− 62.47
KAL-2A	5.09	7.12	− 83.89	1.52	− 66.39
KAL-2B	5.68	5.13	− 84.19	− 0.47	− 66.69
KAL-3	6.60	3.10	− 80.11	− 2.50	− 62.61
KAL-3C	5.21	5.28	− 89.87	− 0.32	− 72.37
KAL-2	5.53	4.76	− 84.30	− 0.84	− 66.80
Dck* > 40%					
KAL-1B	6.04	9.18	− 83.77	3.58	− 66.27
KAL-3A	4.80	6.26	− 88.85	0.66	− 71.35
KAL-3B	4.95	7.78	− 89.62	2.18	− 72.12
KAL-4A	4.45	4.73	89.42	− 0.87	− 71.92
KAL-1C	5.53	6.93	− 94.31	1.33	− 76.81

(*) Calculated for assumed temperature of 200 °C from equations of Sheppard and Gilg (1980) for $\delta^{18}O$ and Gilg and Sheppard (1996) for δD. Dck* = Dickite/(dickite + kaolinite)

pH conditions of hydrothermal fluids should be moderately acidic (approximately pH=4) because of the developments of kaolin group minerals and alunite (Reyes 1990). The pH values of the studied samples are around 5 and correspond to acidic hydrothermal alteration conditions. The acidic condition was the principal control for obstructing the smectite clays, as well as depletion of soluble elements (Na, K, and Ca) ions from ignimbrites (Fig. 9) under an acid leaching environment. The mineralogical composition (dominance with silica and kaolin group minerals, and scarce alunite and jarosite) and pH data indicate typical advanced argillic to argillic alteration conditions under the conditions of moderate to high (150–200 °C) temperature and low pH conditions.

SiO_2 vs. Al_2O_3 relationships between slightly altered and highly altered ignimbrites show a clear geochemical trend from ignimbrite to hydrothermal kaolin transformation (Fig. 10). In addition to this, the broad ranges of Ba and Sr contents of altered ignimbrites are other tools for alteration degree determination (Table 2, Fig. 11). The anomalous increase of these elements in the highest grade altered samples (LOI > 12.5% wt.) should be associated with the grade of hydrothermal alteration as previously mentioned by Dill et al. (1997, 2000). Chondrite normalized LREE contents increase, whereas HREE contents decrease in altered ignimbrites with respect to non-altered ignimbrites. The different contents of REE values for different grades of alterations, such as lower REE values for highly altered ignimbrites, are other geochemical indicators for alteration.

The dominance of kaolinite/dickite, but negligible amounts of illite and mixed-layered illite-smectite minerals, should be controlled by several parameters: (1) low pH and alkalinity conditions of hydrothermal solutions, (2) intense acid leaching, (3) high silica saturation, (4) high-grade activities of ions (H^+, H_4SiO_4, $Al(OH)_4$, etc.) and waters, (5) high dissolution rates of volcanic materials, and (5) composition of volcanic material, i.e., low Fe and/or Mg, whereas high Si and Al, and cation ratios such as K/Na = 0, Si/Al = 1 (Murray 1988; Murray and Keller 1993; Yalçın and Bozkaya 2003; Kadir et al. 2013).

Origin of hydrothermal fluids

The major and trace element geochemical data of altered ignimbrites show a similar composition to non-altered host-rocks, except for somewhat increasing the immobile elements and decreasing mobile elements (Figs. 9, 11, and 12). This data indicates the slight leaching by silica-rich acidic (pH 4–6) hydrothermal solutions. The acidic character of hydrothermal fluids should be derived from silica-rich magmatic fluids which circulated through the acidic pyroclastics rocks with dacite and/or rhyolite composition (Temel 1992; Ertek and Öner 2008).

Acid-rich magmatic vapors seem to be responsible for leaching of the host rock and the advanced argillic alteration. The oxygen and hydrogen isotope data demonstrate that magmatic vapor phases were mixed with meteoric waters for assumed temperature conditions as high as 200 °C (Fig. 13a). The steam-related volcanic environments are the main source responsible for magmatic vapors which circulated along the crack zones within the earliest ignimbrite strata during the approximately 6 Ma duration magmatic period of the Ürgüp formation (Temel 1992).

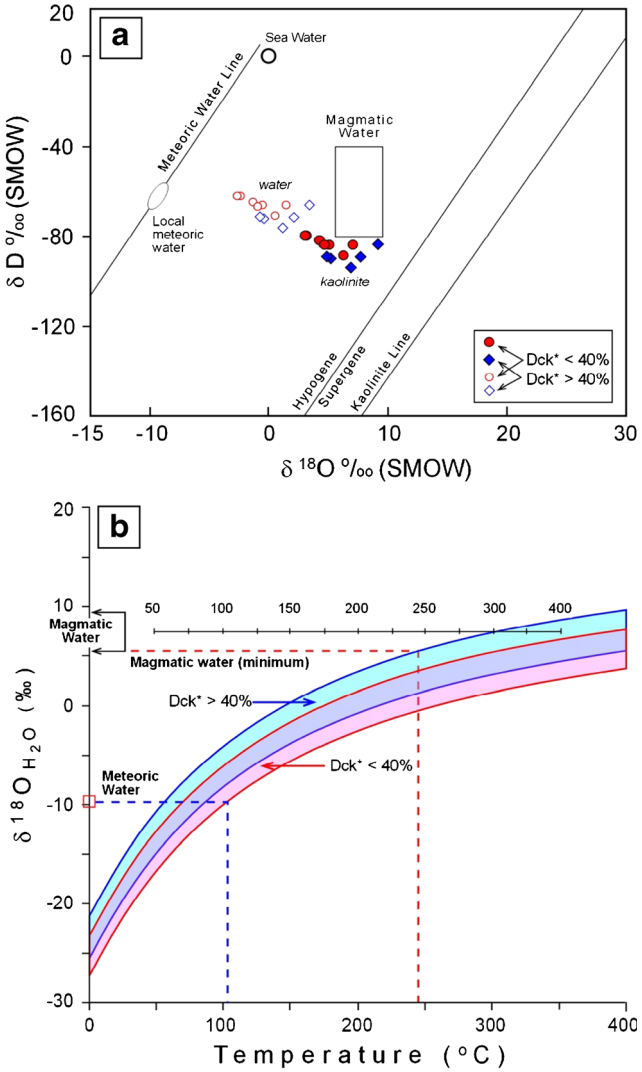

Fig. 13 The distributions of the oxygen and hydrogen isotope data of kaolinite/dickite minerals in $\delta^{18}O$ ‰ vs. δD ‰ diagram (Supergene-hypogene line: Sheppard et al. 1969; kaolinite line: Savin and Epstein 1970; Magmatic water box: Taylor 1979; Local meteoric water is assumed from kaolinite-water equilibrium according to equations of (Savin and Lee 1988 for oxygen and Gilg and Sheppard 1996 for hydrogen). Dck* = dickite/(dickite + kaolinite)

Conclusions

Miocene-Quaternary volcanic complexes associated ignimbrites from the Cappadocia Volcanic Province (CAVP) have been subjected to hydrothermal alteration and produced industrial kaolin group (kaolinite, dickite) clay occurrences. The mineralogical composition of hydrothermally altered samples are represented mainly by quartz and kaolin group clays (kaolinite and dickite), and minor amounts of goethite/limonite, alunite, jarosite, illite, and mixed-layered illite-smectite. Kaolinite, dickite, and quartz, and scarce alunite, jarosite associations suggest that the hydrothermal alteration occurred in acidic (pH < 5) and moderate temperature (approximately 200 °C) conditions, i.e., argillic alteration. The fine-grained kaolinite and dickite and their associations with the fine-grained alunite and jarosite minerals are characteristic for steam-heated related shallow depth environments. Kaolinite and dickite minerals exhibit uniform and prolonged pseudo-hexagonal platelets, respectively, as tightly packed vermicular booklets. Hydrothermal alteration-related silica and kaolin minerals were developed as the mechanism of replacement of volcanic glass/groundmass and neoformation in the pores from the acidic hydrothermal solutions.

The altered samples are classified into three groups based on their loss on ignition values, i.e., slightly, moderately, and highly altered samples. Altered ignimbrites have enrichment for major oxides of TiO_2, Al_2O_3, and P_2O_5, but depletion for SiO_2, MnO, MgO, CaO, Na_2O, and K_2O with respect to host-rock composition. Most of the trace element concentrations were also enriched in altered samples except for Rb, Sr, and P. The noticeable decrease in some elements, such as Rb, K, and Yb, are related element mobility during acidic hydrothermal alteration. Chondrite-normalized REE values show a similar trend but have some differences for altered and host-rock compositions. The contents of LREE increase, but HREE decrease in altered ignimbrites. The oxygen and hydrogen isotope data of kaolinite/dickite demonstrate that magmatic vapor phases mixed with meteoric waters. The steam-heated igneous environment with a duration of 6 Ma seems to be the reason for hot magmatic vapors circulating along the cracks zones through the acidic volcanogenic rocks, and consequently the acidic (low pH) conditions which caused to kaolin-dominant clay alteration.

Acknowledgments I would like to thanks to Ömer Bozkaya (Pamukkale University, Turkey) and to Warren D. Huff (University of Cincinnati, USA), for their careful reading of the manuscript and comments. Their contributions and constructive criticisms significantly improved the manuscript. In this study, the analyses were carried out in the Central Research Laboratory of Ömer Halisdemir University. I would like to thanks to laboratory staffs (Esra Kılavuz, Nebi Yelegen, Zeynep Nalvuran and Sedef Ilk) for their contributions during the analysis. I would like to thanks to anonymous reviewers for their constructive comments and suggestions which improved the paper quality.

References

Aydar E, Gourgaud A (1998) The geology of Mount Hasan stratovolcano, central Anatolia, Turkey. J Volcanol Geotherm Res 85(1-4): 129–152

Aydar E, Schmitt AK, Çubukçu HC, Akin L, Ersoy O, Sen E, Duncan RA, Atici G (2012) Correlation of ignimbrites in the central Anatolian volcanic province using zircon and plagioclase ages and zircon compositions. J Volcanol Geotherm Res 213-214(2012):19–97

Bailey S W (1980) Summary of recommendations of AIPEA nomenclature committee on clay minerals. Am Mineral 65:1–7

Bailey S W (1988) Chlorites: Structures and crystal chemistry. Pp. 347–403 in: Hydrous Phyllosilicates (Exclusive of Micas) (S.W. Bailey,

editor). Reviews in Mineralogy, 19. Mineralogical Society of America, Washington, D.C.

Başıbüyük Z, Yalçın H (2019) Mineralogy, petrography and origin of hydrothermal alteration in Eocene magmatites in Central Anatolia (Sivas-Turkey). M.T.A. Bulletin 158:141–164

Bohor BF, Triplehorn DM (1993) Tonsteins: altered volkanic-ash layers in coal-bearing sequences. Geology Society of American Special Paper, Boulder, p 285

Brown G, Brindley GW (1980) X-ray diffraction procedures for clay mineral identification. Pp. 305-360 in: Crystal Structures of Clay Minerals and their X-ray Identification (G.W. Brindley and G. Brown editors). Mineralogical Society Monograph 5, London,UK.

Craig H (1961) Isotopic Variations in Meteoric Waters. Science 133: 1702–1703

Dill H, Bosse R, Henning H, Fricke A (1997) Mineralogical and chemical variations in hypogene and supergene kaolin deposits in a mobile fold belt the Central Andes of northwestern Peru. Mineral Deposita 32:149–163

Dill HG, Bosse HR, Kassbohm J (2000) Mineralogical and chemical studies of volcanic related argillaceous industrial minerals of the Central American Cordillera (western El Salvador). Econ Geol 95: 517–538

Dunoyer de Segonzac G (1970) The transformation of clay minerals during diagenesis and low-grade metamorphism. A Review. Sedimentology 15:281–326

Ece OI, Ekinci B, Schroeder PA, Crowe D, Esenli F (2013) Origin of the Düvertepe kaolin–alunite deposits in Simav Graben, Turkey: Timing and styles of hydrothermal mineralization. J Volcanol Geotherm Res 255:57–78

Ehrenberg SN, Aagaard P, Wilson MJ, Fraser AR, Duthie DML (1993) Depth-dependent transformation of kaolinite to dickite in sandstones of the Norwegian continental shelf. Clay Miner 28:325–352

Ercan T, Tokel S, Matsuda J, Ul T, Notsu K, Fujitani T (1994) Erciyes Dağı (Orta Anadolu) Pliyo-Kuvaterner volkanizmasina ilşkin yeni jeokimyasal, izotopik, radyometrik veriler ve jeotermal enerji açısından önemi. Türkiye 6. Enerji Kongresi Bildiriler Kitabı, 208–222 (in Turkish).

Ercan HU, Ece OI, Schroeder PA, Karacık Z (2016) Differentiating styles of alteration within kaolin-alunite hydrothermal deposits of Çanakkale, NW Turkey. Clay Clay Miner 64:245–274

Ertek N, Öner F (2008) Mineralogy, geochemistry of altered tuff from Cappadocia (Central Anatolia) and its use as potential raw material for the manufacturing of white cement. Appl Clay Sci 42:300–309

Gilg HA, Sheppard SMF (1996) Hydrogen isotope fractionation between kaolinite and water revisited. Geochim Cosmochim Acta 60:529–533

Guzmán S, Doronzo DM, Marti J, Seggiaro R (2020) Characteristics and emplacement mechanisms of the Coranzulí ignimbrites (Central Andes). Sediment Geol 405:105699

Hedenquist JW, Arribas A Jr, Gonzalez-Urien E (2000) Exploration for epithermal gold deposits. Rev Econ Geol 13:245–277

Hemely JJ (1959) Some mineralogical equilibria in the system K_2O-Al_2O_3-SiO_2-H_2O. Am J Sci 257:241–270

Innocenti F, Mazzuoli R, Pasquare G, Radicati di Brozolo F, Villari L (1975) The Neogene calc-alkaline volcanic of Central Anatolia: geochrono- logical data on Kayseri-Nigde area. Geol Mag 112: 349–360

Inoue A (1995) Formation of clay minerals in hydrothermal environments. In: Velde B (ed) Clays and the Environment: Origin and Mineralogy of Clays. Springer, Berlin, pp 268–329

Kadir S, Erkoyun H (2013) Genesis of the hydrothermal Karaçayır kaolinite deposit in Miocene volcanics and Paleozoic volcanic rocks of the Uşak-Güre basin, western Turkey. Turk J Earth Sci 22:444–468

Kadir S, Gürel A, Senem H, Külah T (2013) Geology of Late Miocene clayey sediments and distribution of palaeosolclay minerals in the northeastern part of the Cappadocian Volcanic Province (Araplı-Erdemli), central Anatolia, Turkey. Turk J Earth Sci 22:427–443

Kadir S, Külah T, Eren M, Önalgil N, Gürel A (2014) Mineralogical and geochemical characteristics and genesis of the Güzelyurt alunite-bearing kaolinite deposit within the Late Miocene Gördeles ignimbrite, central Anatolia, Turkey. Clay Clay Miner 62:486–508

Karakaya N (2009) REE and HFS element behaviour in the alteration facies of the Erenler Dağı Volcanics (Konya, Turkey) and kaolinite occurrence. J Geochem Explor 101:185–208

Karakaya MÇ, Karakaya N, Temel A (2001) Kaolin occurrences in Erenler Dağı volcanics, southwest Konya Province, Turkey. Int Geol Rev 43(8):711–722

Keller WD (1988) Authigenic kaolinite and dickite associated with metal sulfides-probable indicators of a regional thermal event. Clay Clay Miner 36:153–158

Knight JE (1977) A thermodynamic study of alunite, enargite, luzonite, and tennantite deposits. Econ Geol 72:13211336

Koh SM, Chang HW (1997) Comparative anatomy of the hydrothermal alteration of Chonnam and Kyongsang hydrothermal clay alteration areas in Korea. Econ Environ Geol 30:81–87

Le Pennec JL, Bourdier JL, Froger JL, Temel A, Camus G, Gourgaud A (1994) Neogene ignimbrites of Nevşehir Plateau (central Turkey): stratigraphy, distribution and source constraints. J Volcanol Geotherm Res 63:59–87

Le Pennec JL, Temel A, Froger JL, Sen S, Gourgaud A, Bourdier JL (2005) Stratigraphy and age of the Cappadocia ignimbrites, Turkey: reconciling field constraints with paléontologie, radiochronologic, geochemical and paleomagnetic data. J Volcanol Geotherm Res 141:45–64

Marumo K (1989) Genesis of kaolin minerals and pyrophyllite in Kuroko deposits of Japan: implications for the origins of the hydrothermal fluids from mineralogical and stable isotope data. Geochim Cosmochim Acta 53:2915–2924

Mayer K, Scheu B, Montanaro C, Yilmaz TI, Isaia R, Aßbichler D, Dingwell DB (2016) Hydrothermal alteration of surficial rocks at Solfatara (CampiFlegrei): Petrophysical properties and implications for phreaticeruption processes. J Volcanol Geotherm Res 320:128–143

Moore DM, Reynolds RC (1989) X-ray diffraction and the identification and analysis of clay minerals. Oxford University Press, New York, p 332

Mues-Schumacher U, Schumacher R (1996) Problems of stratigraphic correlation and new K-Ar data for ignimbrites from Cappadocia, central Turkey. Int Geol Rev 38(8):737–746

Murray HH (1988) Kaolin minerals: their genesis and occurrences. In: Bailey, S.W. Ed., Hydrous Phyllosilicates exclusive of micas. Mineralogical Society of America. MI Rev Miner 19:67–89

Murray HH, Keller WD (1993) Kaolins. In: Kaolin Geneis and Utilization (eds. H.H. Murray, W. Bundy and C. Harvey). The Clay Mineral Society, Boulder, pp 1–24

Palinkaš SS, Šoštarić SB, Bermanec V, Palinkaš L, Prochaska W, Furić K, Smajlović J (2009) Dickite and kaolinite in the Pb-Zn-Ag sulphide deposits of northern Kosovo (Trepča and Crnac). Clay Miner 44:67–79

Papoulis D, Tsolis-Katagas P (2008) Formation of alteration zones and kaolin genesis, Limnos Island, northeast Aegean Sea, Greece. Clay Miner 43:631–646

Pasquaré G (1968) Geology of the Cenozoic volcanic area of Central Anatolia. Atti Accademei Nazionale dei Lincei Memoire 9:55–204

Reyes AG (1990) Petrology of Philippines geothermal systems and the application of alteration mineralogy to their assessment. J Volcanol Geotherm Res 43:279–309

Ruiz Cruz MD, Reyes E (1998) Kaolinite and dickite formation during shale diagenesis: isotopic data. Appl Geochem 13:95–104

Savin SM, Epstein S (1970) The oxygen and hydrogen isotope geochemistry of clay minerals. Geochim Cosmochim Acta 34:25–42

Sayın SA (2007) Origin of kaolin deposit: evidence from the Hisarcık (Emet-Kütahya) deposits, Western Turkey. Turk J Earth Sci 16: 77–96

Schmitt AK, Danisík M, Evans NJ, Siebel W, Kiemele E, Aydin F, Harvey JC (2011) Acigol rhyolite field, Central Anatolia (part 1): high-resolution dating of eruption episodes and zircon growth rates. Contrib Mineral Petrol 162:1233–1247

Schumacher R, Keller J, Bayhan H (1990) Depositional characteristics of ignimbrites in Cappadocia, Central Anatolia, Turkey. In: Savascin, M.Y., Eronat, A.H. (Eds.), Proc. Int. Earth Sci. Congr. on Aegean Regions, IESCA, 2, pp. 435-449.

Scott KM (1990) Origin of alunite- and jarosite-group minerals inthe Mt. Leyshonepithermal gold deposit, northeast Queensland, Australia. Am Mineral 75:1176–1181

Sheppard SMF, Gilg HA (1996) Stable isotope geochemistry of clay minerals. Clay Miner 31:1–24

Sheppard SMF, Nielsen RL, Taylor HP (1969) Oxygen and hydrogen isotope ratios of clay minerals from porphyry copper deposits. Econ Geol 64:755–777

Simón M, Martin F, Garcia I, Bouza P, Dorronsoro C, Auilar J (2005) Interaction of limestone grains and acidic solutions from the oxidation of pyrite tailings. Environ Pollut 135:65–72

Smith RL (1960) Ash flows. Geol Soc Am Bull 71(6):796–842

Spears DA (2012) The origin of tonsteins, an overview, and links with seatearths, fireclays and fragmental clay rocks. Int J Coal Geol 94:22–31

Sun W, Mc Donough WF (1989) Chemical and isotopic systematics of oceanic basalts: implications for mantle composition and processes. Geol Soc Lond Spec Publ 42:313–345

Taylor HP (1974) The application of oxygen and hydrogen isotope studies to problems of hydrothermal alteration and ore deposition. Econ Geol 69:843–883

Temel A (1992) Kapadokya eksplozif volkanizmasının petrolojik ve jeokimyasal özellikleri. PhD, Hacettepe University, Ankara. Turkey

Temel A, Gündoğdu MN, Gourgaud A, Le Pennec JL (1998) Ignimbrites of Cappadocia (Central Anatolia, Turkey): petrology and geochemistry. J Volcanol Geotherm Res 85:447–471

Viereck-Götte L, Lepetit P, Gürel A, Ganskow G, Çopuroglu I, Abratis M (2010) Revised volcanostratigraphy of the Upper Miocene to Lower Pliocene Ürgüp Formation, Central Anatolian volcanic province, Turkey. In: Gropelli, G., Götte-Viereck, L. (Eds.), Geol Soc Am Spec Pap, 464, 85-112.

Wilson L, Sparks RSJ, Walker GPL (1980) Explosive volcanic-eruptions. 4. The control of magma properties and conduit geometry on eruption column behavior. Geophys J R Astron Soc 63(1):117–148

Wilson CJN, Houghton BF, Kamp PJJ, McWilliams MO (1995) An exceptionally widespread ignimbrite with implications for pyroclastic flow emplacement. Nature 378(6557):605–607

Yalçın H, Bozkaya Ö (2003) Mineralogy and geochemistry of hydrotermal kaolinite and IS occurences, (Yıldızeli-Akdağmadeni) W-Sivas. Geol Bullet Turkey 46, 1-24